RSC Advances

ROYAL SOCIETY OF CHEMISTRY

www.rsc.org/advances

Graphical and textual abstract

Synthesis and self assembly of cystine flowers for applications in biosensing for detection of *Escherichia coli* O157:H7.

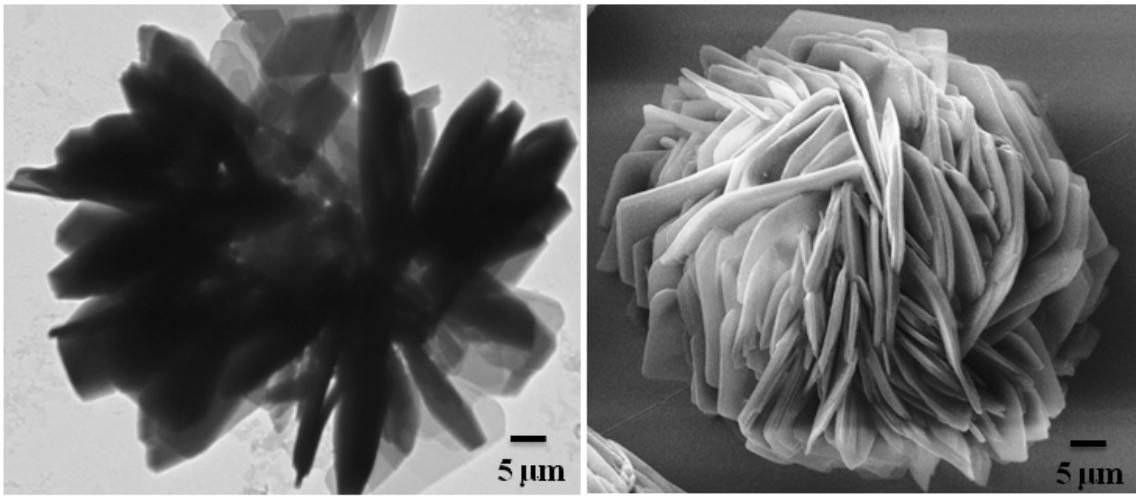

Hierarchical Cystine Flower Based Electrochemical Genosensor for Detection of *Escherichia coli* O157:H7

Chandra Mouli Pandey[ab], Ida Tiwari[b], Gajjala Sumana*[a]
[a]Biomedical Instrumentation Section, CSIR-National Physical Laboratory, New Delhi-110012, India
[b]Department of Chemistry, Faculty of Science, Banaras Hindu University, Varanasi-221005, India

Abstract

Here, we report a simple and re-producible method for large scale fabrication of novel organic flowers of cystine (CysFl) with high uniformity, at controlled pH and concentration. These 3D flowers like structures have purely hierarchic arrangement, wherein each petal is composed of several cystine molecules with the average size of 50 μM, as determined by transmission electron microscopy. The CysFl was self-assembled onto gold electrode and has been utilized to serve as matrices for covalent immobilization of *Escherichia coli* O157:H7 (*E. coli*) specific probe oligonucleotide, identified from the 16s rRNA coding region of the *E. coli* genome. This fabricated CysFl platform is sought to provide improved fundamental characteristics to the electrode interface in terms of electro-active surface area, diffusion coefficient, and electron transfer kinetics. Electrochemical impedance spectroscopy reveals that this genosensor exhibits a linear response to complementary DNA in the concentration range of 10^{-6} to 10^{-15} M with a detection limit of 1×10^{-15} M. Under optimal conditions, this biosensor is found to retain about 88 % of the initial activity after 6 cycles of use.

Keywords: Cystine, Organic flowers, Genosensor, Electrochemical impedance spectroscopy, *Escherichia coli*.

***Corresponding author:** sumanagajjala@gmail.com; Tel.: +91-11-45609152

1. Introduction

Micro-organisms such as bacteria and virus, are widely found in food, soil, water and the intestinal tracts of humans and animals.[1] Some of these micro-organisms play a crucial function in nature, but some potentially harmful micro-organisms can have intense negative effects on both animals and humans.[2] Among them, entero-hemorrhagic *Escherichia coli* (*E. coli* O157:H7) is a major food-borne and waterborne pathogen which causes diarrhea, hemorrhagic colitis, and hemolytic uremic syndrome.[3, 4] The traditional method reported for the detection of *E. coli* O157:H7 in food and water, includes cultures using selective media,[5] serotyping[6, 7] and PCR amplification.[8, 9] Though, these methods are of high accuracy, but the operating procedure involved is complex, time-consuming and some techniques have limited sensitivity and specificity.[10] Hence, it is necessary to fabricate a sensitive, specific and rapid detection technique for *E. coli* which has implications in environmental monitoring, food industry and clinical chemistry. Currently, surface Plasmon resonance,[11] quartz crystal microbalance,[12] and electrochemical[13, 14] transduction techniques have been proposed as substitute to these conventional methods. And among them, electrochemical nucleic acid biosensor has evoked considerable interest because of its unique properties of simplicity, rapidity, accuracy, low cost and portability.[15, 16] Electrochemical biosensors detect the nucleic acid binding events on solid-state transducer surface by monitoring the electrochemical spectrum change.[16-18]

In the fabrication of high performance biosensors for clinical diagnostics, the structure, morphology of the matrices and the immobilization of bio-analytes for achieving rapid and sensitive detection of bio-recognition is a major challenge.[19] In view of the motivating phenomena occurring at ordered microstructures and nanoscale materials, significant work has recently been directed in the synthesis of novel materials and exploring their application for variety of vital fields including catalysis, point of care diagnostics for infectious diseases and therapeutics.[20,21,13] Presently, the applications of nano-materials have been widely used as a signal amplification medium to enhance the limit of DNA detection.[22, 23] In this context, the synthesis of polyaniline nanotubes, has been reported that can detect the nucleic acid with a detection limit of 1.0 fM.[24] The fabrication of a nanoporous gold electrode using encoded gold nanoparticles achieved a

detection limit of about 28 aM.[25] A label-free DNA sensor was also prepared using gallium nitride nanowires which revealed picomolar concentration of target DNA.[26] Wang et al. have fabricated a gold nanoflower modified electrochemical DNA biosensor showing the detection of target DNA with a detection limit of 1 pM.[27] There are reports on the modification of electrode by different nanomaterials to improve DNA detection but the strategies adopted for these modifications are relatively complex. The modification of the surface using surfactant or polymer matrix in the preparation and assembly of nanomaterials often causes some vague effects in DNA detection.[28] Thus, there is necessity for the construction of nanostructure modified electrode by a simple strategy for improved and sensitive detection of DNA. In this context, very few reports are available on the application of hierarchical structures of organic and related compounds for fabrication of nucleic-acid biosensors. These hierarchically structured materials not only possess structural organization at various scales but they also leads to the improved material properties and performance in terms of high surface area, synergistic interactions, and multiple functionalities.[29, 30] Further, the ability to design these hierarchically structures from materials with a self-assembling properties at the nanometer scale opens new opportunities for application in the field of biosensors.[31, 32]

Previously, we have reported the detection of nucleic acid using micro-structured cystine dendrites, wherein the role of functional groups and morphology of dendritic cystine was discussed.[33] However, there is a lot of scope in tailoring of the order and morphology of the amino acid for enhancing the sensitivity and stability of the biosensor. Therefore, in the present work detailed experiments have been carried out to explore the complexation efficiencies for DNA strands binding with probe molecules, immobilized on cystine flowers (CysFl). These CysFl are being considered as model system due to its intriguing properties such as ease of preparation, less chemical handling, and they have a common functionality at one end of the molecule, coupled to a range of gradually differentiated functionalities at the other. Further, this CysFl has been utilized to fabricate a label free electrochemical genosensor by covalently immobilizing specific probe oligonucleotide, identified from the 16s rRNA coding region of the *E. coli* genome. These CysFl based platform was found to possess increased electro-active surface area

and high electron transport at the electrode-electrolyte interface, thus enhancing the sensitivity of the genosensor.

2. Materials and Methods

2.1. Chemicals and oligonucleotides. L-Cysteine (analytical grade, 98.5%), N-hydroxysuccinimide (NHS), N-ethyl-N-(3-dimethylaminopropyl carbodimide) (EDC), and all other reagents and solvents have been procured from Sigma-Aldrich (India). Probe sequence specific to *E. Coli*, identified from the 16s rRNA coding region of the *E. coli* genome, complementary, non-complementary and one-base mismatch target sequences have been procured from Sigma Aldrich, Milwaukee, USA and are as follows.[13]

DNA probe:	NH_2-5´-GGT CCG CTT GCT CTC GC-3´
Complementary:	5´-GCG AGA GCA AGC GGA CC-3´
Non-complementary:	5´-CTA GTC GTA TAG TAG GC-3´
One-base mismatch:	5´-GCG AGA G**A**A AGC GGA CC-3´

The bacterial culture samples of other water borne pathogens have been provided by All India Institute of Medical Sciences (AIIMS), New Delhi, India. The solutions of oligonucleotide are prepared in Tris–EDTA buffer (1M Tris–HCl, 0.5M EDTA) of pH 8.0 and stored at -20^{o}C prior to use.

2.2. Synthesis of cystine flowers (CysFl). For the synthesis of CysFl, 100 mM L-Cysteine aqueous solution was prepared by maintaining the pH at 8.0 using sodium carbonate. The solution was sonicated for 30 min at 25^{o}C, using ultra sonic bath and the crystal growth of CysFl was observed by keeping the solution at 25^{o}C for 12 h. For TEM analysis, the prepared CysFl was dropped onto carbon grid and dried at room temperature.

2.3. Fabrication of CysFl/Au electrode. The gold (Au) electrode (0.5 cm^2 diameter) was washed in boiling 2.0 M KOH for about 1 h, following ultra-sonication in Piranha solution (3:1 H_2SO_4/H_2O_2) for 10 min. The electrode is voltammetrically cycled and characterized in 0.2 M H_2SO_4 (-0.5 V to -1.4 V vs.Ag/AgCl) with scan rate of 0.10 V/s until a stable cyclic voltammogram is obtained. Self assembly of CysFl is achieved by dipping pre-cleaned gold electrode into 100 mM CysFl solution overnight (12 hrs) at

27^{o}C. After that, the electrodes were taken out and washed repeatedly with de-ionized water.

2.4. Immobilization of probe DNA and hybridization with target DNA. The fabricated CysFl/Au electrode was activated using EDC (2mM) and NHS (5mM) and kept for 1 hr in dark. Subsequently 40µl of pDNA (10^{-6} M) was immobilized onto the modified electrode at 100% humidity at room temperature (~27^{o}C) for about 6 h followed by rinsing with tris-HCl. The hybridization studies have been performed as a function of target DNA concentration with complementary, non-complementary and one-base mis-match sequences in a humid chamber for about 20 min at 35^{o}C. The proposed mechanism for the synthesis of CysFl and the fabrication of nucleic acid sensor for *E. coli* detection is shown in Scheme1.

2.5. Extraction of DNA from bacterial clinical samples. The extraction of DNA has been conducted from a panel of strains comprising of *E. coli*, *Salmonella typhimurium*, *Neisseria meningitides*, and *Shigella dysenteriae.* For this process, the suspensions of the colonies were vortexed by pouring it into 100 µl sterile MilliQ water. The suspension is boiled for 10 minutes and is centrifuged at 10, 000 rpm for 5 min, followed by the addition of equal volume (100 µl) of 24:1 (v/v) chloroform: iso-amyl alcohol. Solution was again centrifuged (12000 rpm, 10 mins), which result in the formation of aqueous layer containing DNA which was carefully pipetted out and kept at -20^{o}C prior to use.[33]

2.6. Pre-treatment of extracted DNA. All the bacterial clinical samples are prepared in Tris-EDTA buffer and are denatured by heating in a water bath (95°C) for 5 min and are immediately chilled in ice to obtain denatured single-stranded DNA. These aliquot of samples are subjected to sonication (15 min at 120 V) to break the long DNA strands into smaller fragments of the DNA.[2]

2.7. Characterization. Structural and morphological investigations of CysFl have been carried out using X-ray diffraction (XRD, Cu Kα radiation, Rigaku, miniflax 2) and transmission electron microscopic (TEM, Hitachi Model, H-800) studies. The scanning electron microscopic (SEM) images have been recorded using a JEOL-JSM-6700F field-emitting scanning electron microscope (FESEM, 15 kV). Contact angle (CA) measurements have been taken using contact angle meter (Data Physics OCA15EC). Fourier transform infra-red (FT-IR) spectroscopy measurements have been carried out

using Perkin-Elmer spectrometer (Model Spectrum BX) at 25^{o}C. Electrochemical analysis has been carried out on an Autolab potentiostat/galvanostat (Eco Chemie, Netherlands) using a three-electrode cell with Au as working electrode, platinum as auxiliary electrode and Ag/AgCl as reference electrode in phosphate buffer saline (PBS, 100 mM, pH 7.0, 0.9% NaCl) containing 5 mM $[Fe(CN)_6]^{3-/4-}$.

3. Results and discussion

3.1. Characterization of CysFl. The powder XRD pattern of CysFl is displayed in figure 1A. The main diffraction peaks of CysFl structures appear at 18.8^{o}, 28.4^{o}, 33.0^{o} and 34.3^{o} corresponds to 100, 001, 112, and 116 respectively. The diffraction peaks shows a pure hexagonal phase, which is in good agreement with the standard value for the bulk hexagonal L-cystine (JCPDS 261776).[33,34] FTIR spectroscopy has been used to characterize CysFl and pDNA/CysFl/Au electrode in the frequency region from 400-1800 cm^{-1}. The characteristic bands of CysFl seen at 1490 cm^{-1} is due to the presence of amino groups. An intense absorption peaks at 1590 cm^{-1}, 1624 cm^{-1} and1420 cm^{-1}, 1490 cm^{-1} may be assigned to the asymmetric deformation of NH_3^+ and asymmetric stretching of COO^- respectively. Bands seen at 1420 cm^{-1}, 1295 cm^{-1} and 782 cm^{-1} are attributed to CH_2-CO deformation, CH_2 wagging and rocking vibrations respectively confirming the presence of CH_2 group (Fig. 1B).[32,33] After the immobilization of pDNA on CysFl the nitrogen base region (1700-1500 cm^{-1}) in the DNA spectrum overlaps with the amine signals of CysFl. The absorption bands seen at 1330 and 1133 cm^{-1} may be assigned to the anti-symmetric and symmetric stretching vibration of the phosphate groups, respectively (Fig. 1C). Further, the IR absorption peak at 1048 cm^{-1} is due to the vibration of ribose (C-C sugar) and absorption at 903 cm^{-1} is an indication for the immobilization of DNA on the surface of CysFl.

3.2. Microscopic analysis of the CysFl. TEM studies have been carried out to study the formation of CysFl. Figure 2A shows that the CysFl consist of several hexagonal structures arranged in an ornate manner, where the size of each flower is 50 μM. High resolution TEM image shows that the thickness of each hexagonal flake is about 1 μM (Fig. 2B) and they are arranged facial to each other. TEM studies reveal that the growth of these CysFl starts with the formation of cystine hexagons and with increase in the reaction time, these primary hexagonal cystine crystals agglomerate together and result in

the formation of flower like structures.[32] The formation of these structures can be attributed to acoustic cavitations, and the mechanism is described elsewhere.[33] It appears that the intermolecular electrostatic interactions of hydrogen bonding are responsible for the formation of CysFl which depends on the change in pH.[35]

3.3. Morphological characterization of the CysFl/Au and pDNA/CysFl/Au electrodes. The surface morphological studies of CysFl/Au and DNA/CysFl/Au bioelectrode have been investigated using SEM. Figure 3A shows the self assembly of CysFl onto gold surface, where the assemblies are formed in isolation and do not connect among themselves. The high magnification image shows that each flower consists of several hexagonal flakes arranged in a patterned manner (Fig. 3A, inset). After the immobilization of pDNA, on CysFl/Au electrode, shiny and fibrous morphology is observed (Fig. 3B). This increase in chemically accessible area may be due to well-oriented functional groups present in the CysFl which help in the covalent binding of the amino terminated pDNA.

3.4. Contact Angle Studies (CA) for Au, CysFl/Au and pDNA/CysFl/Au electrodes. To investigate pDNA/CysFl/Au bioelectrode fabrication, the CA measurements were carried out using the sessile drop method. The change in the value of the contact angle reveals the hydrophobic/hydrophilic character of the surface, which in turn can be related to CysFl self assembly and pDNA immobilization on CysFl/Au electrode. Table S1 shows the CA data of bare Au, CysFl/Au and pDNA/CysFl/Au bioelectrodes respectively. It can be seen that the value of the CA decreases after the self assembly of CysFl (Fig. 4B) onto Au electrode (Fig. 4A) indicating the presence of large number of hydrophilic functional group (-COOH, -NH_2 and -SH) in CysFl. The CA measurements were also performed to confirm the immobilization of pDNA onto CysFl/Au electrode, and it was found that with the progress of immobilization process, the surface becomes more hydrophilic, owing to presence of the phosphodiester backbone of pDNA. The CA value subsequently decreases with time (4-18 h) and becomes constant at 29.65° (Fig. 4C) after about 6 h revealing that complete immobilization of probe occurs in this duration.

3.5. Electrochemical characterization

3.5.1. Electrochemical impedance spectroscopy studies. Electrochemical impedance spectroscopic (EIS) is a powerful and sensitive tool for studying the charge transfer processes occurring at electrode-solution or modified electrode-solution interfaces.[36] In the Nyquist plot of the impedance spectra, semicircle corresponds to the electron transfer resistance process (R_{ct}) which usually depends on the dielectric and insulating features at the electrode-electrolyte interface.[37, 38]

Figure 5 shows the EIS studies of CysFl/Au electrode, EDC/NHS activated CysFl/Au electrode and pDNA/CysFl/Au bioelectrode in phosphate buffer (100 mM, pH 7.0, 0.9% NaCl) containing 5mM $[Fe(CN)_6)]^{3-/4-}$ as a redox marker. The equivalent circuit (Fig. 5, inset) and the calculated values for solution resistance (R_s), constant phase element (C_{PE}), and warburg impedance **(**W) value corresponding to different modifications are given in Table S2. The impedance spectra are composed of a semi-circle slightly shifted from the origin for all the concentrations in solution. The low frequency semi-circle is characteristic of an interfacial charge transfer reaction. The surface modification of the Au electrode with CysFl results in the increase of the R_{ct} value (250.4 Ω, curve (i)). This increase in R_{ct} value is due to the presence of negative charges from $–COO^-$ groups of CysFl that interrupt the interfacial electron-transfer rate between the electrode and the electrolyte solution. Interestingly, when CysFl/Au electrode was activated with EDC/NHS, there was a decrease in the R_{ct} value which may probably be due to the blocking of negative charges of $–COO^-$ groups of CysFl, and the available of net positive charges attract negative redox marker, resulting in decrease of R_{ct} (16.7 Ω, curve iv).[33] When the pDNA was immobilized on CysFl/Au electrode there was an increase in the R_{ct} value (47.54 Ω, curve iii) which could be ascribed to the repellence of redox probe from approaching electrode surface by negative-charged phosphate skeletons of DNA. Further, when the pDNA is incubated with its cDNA sequence, the hybridization process occurs and more negatively charged phosphate backbones are introduced resulting in the increase of R_{ct} (149.3 Ω, curve ii).

3.5.2. Cyclic voltammetry studies. To investigate the various kinetic parameters, cyclic voltammograms of pDNA/CysFl/Au electrode were recorded as a function of scan rate (10-300 mV/s). It was seen that the magnitude of electrochemical response current

[anodic (I_{pa}) and cathodic (I_{pc}), Fig. S1A] for the bioelectrodes and is linearly dependent on the scan rate and follows eqs. (1) and (2). The separation of peaks suggests that the process is not perfectly reversible; however, stable redox peak current and position during repeated scans at a particular scan rate suggests that CysFl based electrodes exhibit a quasi-reversible process.[37] Also it was noted that, the magnitude of both anodic (E_a) and cathodic peak (E_c) potentials (Fig. S1B) increases linearly as function of scan rate (Eqs. (3) & (4)) which reveals that, the electron transport from redox moieties to the electrode is very facile.

I_{pa} (A) [pDNA/CysFl/Au] = 4.8957×10^{-5} (A) + 5.3112×10^{-5} A (s/mV) [scan rate (mV/s)]

R = 0.9986, SD = 1.208×10^{-5} (1)

I_{pc} (A) [pDNA/CysFl/Au] = -1.1785×10^{-4} (A) – 3.542×10^{-5} A (s/mV) [scan rate (mV/s)]

R = 0.9920, SD = 1.8612×10^{-5} (2)

E_a (V) [pDNA/CysFl/Au] = 0.1302 (V) + 0.4606 (V) *Log [scan rate]

R = 0.9776, SD = 0.0043 (3)

E_c (V) [pDNA/CysFl/Au] = 0.1181 (V) – 0.0384 (V) *Log [scan rate]

R = 0.9885, SD = 0.0025 (4)

On the basis of the linear slope of the anodic peak currents on the square root of potential sweep rates (Fig. S1B), it is obvious that the ions transport from bulk to the electrode surface occurs exclusively by diffusion.[39] Further, the diffusion coefficient is calculated by a concentration gradient of $[Fe(CN)_6)]^{3-/4-}$ ions between bulk and interface which can be calculated using the Randles−Sevick equation:

$$I_p = (2.99 \times 10^5)\, \alpha^{1/2}\, n^{3/2}\, ACD^{1/2}\, \upsilon^{1/2} \quad (5)$$

the diffusion coefficient for the pDNA/CysFl/Au electrode is calculated to be 7.19×10^{-6} $cm^2\ s^{-1}$ and for the CysFl/Au electrode it was found to be 1.02×10^{-5} $cm^2\ s^{-1}$. From the above kinetics calculation it can be inferred that the CysFl/Au assembly is sought to provide improved electron transfer kinetics to the electrode interface.

3.6. Electrochemical response studies

3.6.1. Response Studies of pDNA/CysFl/Au bioelectrode. The sensitivity of the pDNA/CysFl/Au bioelectrode has been investigated using EIS by varying the cDNA concentration from 10^{-6} M to 10^{-15} M (Fig. 6A). It was found that with change in cDNA concentration, there was change in R_{ct} value. This signify that the hybridization reaction

is occurring at the bioelectrode due to which there is more accumulation of negatively charged phosphate backbones, hence the R_{ct} value increases following the formation of double stranded DNA. The difference ($\Delta R_{ct} = R_{ct(cDNA)} - R_{ct(pDNA)}$) between the value of the pDNA immobilized electrode and that after hybridization with cDNA has been used as the measurement signal. The analytical signal (ΔR_{ct}) shows linear relationship with the logarithmic value of the complementary target DNA concentration ranging from 10^{-15} to 10^{-6} M (Fig. 6B) and follows Eq. 6:

$$\Delta R_{ct} = 161.47 + 9.07 \log cDNA \quad (6)$$

with linear regression coefficient of 0.998. The detection limit is calculated to be 1×10^{-15} M using the expression 3σ, where σ was estimated as the standard deviation (n = 10) of the impedimetric signals obtained in the absence of bacteria. As CysFl contain ample of functional group for the immobilization of biomolecule, more number of pDNA is immobilized onto the CysFl/Au electrode leading to the enhancement in the hybridization efficiency. In this case, the pathway of electron transfer to/from the electrode was very effectively blocked and changes in R_{ct} values were remarkably enhanced upon hybridization leading to a low detection limit. Further, the association constant (K_a) between cDNA and pDNA/CysNf/Au bioelectrode has been estimated from the slope of the regression equation and found to be 0.243 M^{-1} (Fig. S2).[40, 41] The performances of the DNA hybridization detection based on pDNA/CysFl/Au platform were compared with other hierarchical structures based biosensor, as shown in Table 1. It has been observed that CysFl based platform had lower detection limit and wider detection range for nucleic acid detection.

3.7. Selectivity of the bioelectrode

The specificity of the pDNA/CysFl/Au bioelectrode towards different target DNA sequences (complementary, non-complementary and one base mismatch) and culture samples of *E. coli*, *S. Typhimurium*, *N. Meningitidis* and *S. Dysenteriae* has been studied using EIS (Fig. 7). After incubation of the bioelectrode with *E. coli* spiked and *E. coli* culture DNA there was a marked increase in the semicircle diameter and the R_{ct} value was nearly same to that of cDNA, showing the process of hybridization. When the pDNA/CysFl/Au bioelectrode is incubated with non-complementary and culture samples of bacterial pathogens DNA, there was a slight or negligible change in the R_{ct} value with

respect to the pDNA. Since, the non-complementary DNA bases do not match with the pDNA bases it is expected that there is no hybridization taking place and hence the R_{ct} should result in a semicircle diameter similar to that of pDNA/CysFl/Au bioelectrode (Fig. 7, inset).[33] A slight increase in R_{ct} for *S. Typhimurium* and *N. Meningitidis* DNA has been observed which may perhaps be due to nonspecific DNA interaction with the pDNA/CysFl/Au bioelectrode surface leading to an increase in negative charges on the electrodes surface. When the pDNA/CysFl/Au bioelectrode is exposed to the one base mis-match DNA sequence there was a slight increase in semicircle diameter in comparison to that of the pDNA. This may be due to the partial hybridization of pDNA with the complementary bases of the one base mis-match DNA resulting in increased negative charge of the electrode surface due to higher blocking effect of the surface or repulsion of marker ion.[19] These results reveal that the fabricated genosensor based on CysFl/Au platform is highly specific for the detection of *E. coli* O157:H7.

3.8. Reusability and stability of the bioelectrode

The strong binding of pDNA with the CysFl/Au electrode surface shows the stability of the genosensor to allow for ready regeneration. For this, the electrode was immersed into a buffer solution (pH 8.0) containing Tris−HCl (10 mM) and EDTA (1 mM) at 100 °C for 5 min, followed by cooling in the ice bath for about 30 min, which completely removes cDNA via thermal denaturation.[39] The R_{ct} value of the genosensor has been found to decrease after each regeneration process with an average signal loss of about 2 % (Table S3). This reduction in signal may be possibly due to surface fouling during the regeneration process. The total loss of hybridization signal after 6 cycles is about 15.4 Ω, and it corresponds to ~11.37 % loss of the initial value, indicating that the bioelectrode reproducibly detects target DNA over repeated uses (Fig. 8A). To investigate the storage stability of the fabricated sensor, five measurements have been recorded each week for over 30 days of continuous analysis. The decrease in signal response of the bioelectrode observed was less than 10% when stored at 4 °C (Fig. 8B).

4. Conclusions

In summary, the present work emphasizes the synthesis of cystine flowers prepared using acoustic cavitation method and its application towards *E. coli* detection. The structural and morphological studies have given the strong evidence for the

formation of CysFl and its self assembly onto gold electrode. Label-free detection using electrochemical impedance spectroscopic technique reveals that the fabricated biosensor with an appropriately optimized protocol can accurately detect *E. coli* in the range of 10^{-6} to 10^{-15} M. This fabricated biosensor is found to be selective for *E. coli* detection and retains significant activity (88 % of the initial activity) after 6 cycles of use. It should be interesting that our sensing strategy would be extended for determination of other micro-organisms and open new avenues for the design of electrochemical nucleic acid sensors.

Acknowledgements

We thank Prof. R.C.Budhani Director, CSIR-NPL, New Delhi, India for the facilities. C.M.P. is thankful to CSIR, India, for the award of SRF. We thank Dr. A.M.Biradar (NPL, New Delhi), Prof. B.D.Malhotra (DTU, Delhi) and Dr. A.K.Pandey (PGIMER, Chandigarh) for interesting discussions. Thanks are due to Dr. Seema Sood (AIIMS, New Delhi) for providing the bacterial culture samples. The financial support received from DST, (Grant No. DST/TSG/ME/2008/18) India is gratefully acknowledged.

References

1. P. Leonard, S. Hearty, J. Brennan, L. Dunne, J. Quinn, T. Chakraborty and R. O' Kennedy, *Enzyme Microb. Technol.* 2003, 32, 3-13.
2. C. M. Pandey, R. Singh, G. Sumana, M. K. Pandey and B. D. Malhotra, *Sensor Actuat. B-Chem.* 2011, 151, 333-340.
3. H. Karch, P. I. Tarr and M. Bielaszewska, *Int. J. Med. Microbiol.* 2005, 295, 405-418.
4. J. G. Wells, B. R. Davis, I. K. Wachsmuth, L. W. Riley, R. S. Remis, R. Sokolow and G. K. Morris, *J. Clin. Microbiol.* 1983, 18, 512-520.
5. T. S. Hammack, P. Feng, R. M. Amaguana, G. A. June, P. S. Sherrod and W. H. Andrews, *Journal of AOAC International*, 1997, 80, 335-340.
6. P. A. Chapman, A. T. Malo, C. A. Siddons and M. Harkin, *Appl. Environ. Microbiol.* 1997, 63, 2549-2553.
7. J. Czajka and C. A. Batt, *J. Appl. Microbiol.* 1996, 81, 601-607.
8. J. A. Higgins, S. Nasarabadi, J. S. Karns, D. R. Shelton, M. Cooper, A. Gbakima and R. P. Koopman, *Biosens. Bioelectron.* 2003, 18, 1115-1123.

9. G. Wang, C. G. Clark and F. G. Rodgers, *J. Clin. Microbiol.* 2002, 40, 3613-3619.
10. X. Jiang, K. Chen, J. Wang, K. Shao, T. Fu, F. Shao, D. Lu, J. Liang, M. F. Foda and H. Han, *Analyst*, 2013, 138, 3388-3393.
11. A. D. Taylor, Q. Yu, S. Chen, J. Ã. Homola and S. Jiang, *Sensor Actuat. B-Chem.* 2005, 107, 202-208.
12. X. Mao, L. Yang, X.-L. Su and Y. Li, *Biosens. Bioelectron.* 2006, 21, 1178-1185.
13. C. M. Pandey, A. Sharma, G. Sumana, I. Tiwari and B. D. Malhotra, *Nanoscale*, 2013, 5, 3800-3807.
14. P. Geng, X. Zhang, Y. Teng, Y. Fu, L. Xu, M. Xu, L. Jin and W. Zhang, *Biosens. Bioelectron.* 2011, 26, 3325-3330.
15. N. Prabhakar, K. Arora, S. K. Arya, P. R. Solanki, M. Iwamoto, H. Singh and B. D. Malhotra, *Analyst*, 2008, 133, 1587-1592.
16. J. Wang, *Anal. Chim. Acta.* 2002, 469, 63-71.
17. A. Bonanni and M. del Valle, *Anal. Chim. Acta.* 2010, 678, 7-17.
18. C.-z. Li, H. Karadeniz, E. Canavar and A. Erdem, *Electrochim. Acta*, 2012, 82, 137-142.
19. B. Chen, Y. Xiao, C. Liu, C. Li and F. Leng, *Nucleic Acids Res.* 2010, 38, 3643-3654.
20. J. Wang, G. Rivas, X. Cai, M. Chicharro, C. Parrado, N. Dontha, A. Begleiter, M. Mowat, E. Palecek and P. E. Nielsen, *Anal. Chim. Acta.* 1997, 344, 111-118.
21. P. Wagner, M. Hegner, P. Kernen, F. Zaugg and G. Semenza, *Biophys. J.* 1996, 70, 2052-2066.
22. J. Wang, *Anal. Chim. Acta.* 2003, 500, 247-257.
23. A. Erdem, *Talanta*, 2007, 74, 318-325.
24. H. Chang, Y. Yuan, N. Shi and Y. Guan, *Anal. Chem.* 2007, 79, 5111-5115.
25. K. Hu, D. Lan, X. Li and S. Zhang, *Anal. Chem.* 2008, 80, 9124-9130.
26. C.-P. Chen, A. Ganguly, C.-H. Wang, C.-W. Hsu, S. Chattopadhyay, Y.-K. Hsu, Y.-C. Chang, K.-H. Chen and L.-C. Chen, *Anal. Chem.* 2008, 81, 36-42.
27. L. Wang, X. Chen, X. Wang, X. Han, S. Liu and C. Zhao, *Biosens. Bioelectron.* 2011, 30, 151-157.

28. N. Singh, B. Manshian, G. J. S. Jenkins, S. M. Griffiths, P. M. Williams, T. G. G. Maffeis, C. J. Wright and S. H. Doak, *Biomaterials*, 2009, 30, 3891-3914.
29. Z. Ren, Y. Guo, C.-H. Liu and P.-X. Gao, *F.Chem.* 2013, 1, 18.
30. M. Byun, N. B. Bowden and Z. Lin, *Nano Letters*, 2010, 10, 3111-3117.
31. Y.-P. Zhu, T.-Z. Ren, T.-Y. Ma and Z.-Y. Yuan, *Int J Photoenergy* 2014, 2014, 15.
32. C. M. Pandey, G. Sumana and I. Tiwari, *Biosens. Bioelectron.* 2014, 61, 328-335.
33. C. M. Pandey, G. Sumana and B. D. Malhotra, *Biomacromolecules*, 2011, 12, 2925-2932.
34. J. D. Rimer, Z. An, Z. Zhu, M. H. Lee, D. S. Goldfarb, J. A. Wesson and M. D. Ward, *Science*, 2010, 330, 337-341.
35. H. Hongliang, W. Chungang, M. Zhanfang and S. Zhongmin, *Nanotechnology*, 2006, 17, 5163.
36. F. Lisdat and D. SchÃ¤fer, *Anal. Bioanal. Chem.* 2008, 391, 1555-1567.
37. A. Kaushik, A. Vasudev, S. K. Arya and S. Bhansali, *Biosens. Bioelectron.* 2013, 50, 35-41.
38. A. Kaushik, P. R. Solanki, K. Kaneto, C. G. Kim, S. Ahmad and B. D. Malhotra, *Electroanalysis*, 2010, 22, 1045-1055.
39. A. Sharma, G. Sumana, S. Sapra and B. D. Malhotra, *Langmuir*, 2013, 29, 8753-8762.
40. I. Szymanska, H. Radecka, J. Radecki and R. Kaliszan, *Biosens. Bioelectron.* 2007, 22, 1955-1960.
41. S. K. Arya, T. S. Pui, C. C. Wong, S. Kumar and A. R. A. Rahman, *Langmuir*, 2013, 29, 6770-6777.
42. X. Wang, T. Yang, X. Li and K. Jiao, *Biosens. Bioelectron.* 2011, 26, 2953-2959.
43. Y. Hu, S. Hua, F. Li, Y. Jiang, X. Bai, D. Li and L. Niu, *Biosens. Bioelectron.* 2011, 26, 4355-4361.

Figure Captions

Scheme 1. Schematic showing the synthesis and fabrication of CysFl and pDNA/CysFl/Au bioelectrode.

Figure 1. (A) X-ray diffraction pattern of CysFl. FT-IR spectra of (A) CysFl/Au electrode, and (B) pDNA/CysFl/Au bioelectrode.

Figure 2. TEM image **(A)** showing the formed CysFl at pH 8.0 and 100 mM concentration and **(B)** the arrangement of hexagonal petals in CysFl.

Figure 3. SEM image of **(A)** denCys/Au electrode, and **(B)** pDNA/denCys/Au bioelectrode.

Figure 4. Contact angle studies of **(A)** Au electrode, **(B)** CysFl/Au electrode, and **(C)** pDNA/CysFl/Au bioelectrode.

Figure 5. EIS showing the Nyquist diagram (Z_{im} versus Z_{re}) for the Faradic impedance measured in 5 mM $[Fe(CN)_6]^{3-/4-}$ PBS solution at pH 7.0 in the frequency for 10^5 Hz to 0.1 Hz (i) CysFl/Au electrode (ii) complementary DNA incubated on pDNA/CysFl/Au bioelectrode (iii) pDNA/CysFl/Au bioelectrode (iv) EDC/NHS activated CysFl/Au electrode.

Figure 6. EIS response of **(A)** pDNA/CysFl/Au bioelectrode as a function of cDNA concentration (10^{-6}-10^{-15} M) in 5 mM $[Fe(CN)_6]^{3-/4-}$ PBS solution at pH 7. **(B)** Plot of the ratio of charge transfer resistance after and before hybridization, R_{ct} target/R_{ct} pDNA, of the pDNA/CysFl/Au bioelectrode vs. the logarithm of the target DNA concentrations.

Figure 7. Bar diagram indicating the specificity of the bioelectrode w.r.t. change in R_{ct} values for (i) spiked *E. coli* (ii) cDNA (iii) *E. coli* cultured (ii) one base mismatch (iii) *S. Typhimurium* (iv) *N. Meningitidis* (v) non complementary (iv) *S. Dysenteriae* immobilized onto (v) pDNA/CysFl/Au bioelectrode. Inset figure shows the Nyquist plots for the different cultured sample immobilized onto pDNA/CysFl/Au bioelectrode in 5 mM $[Fe(CN)_6]^{3-/4-}$ PBS solution at pH 7.

Figure 8. (A) The percentage change in R_{ct} of the fabricated pDNA/CysFl/Au bioelectrode towards *E. coli* detection was determined after each regeneration cycle (6 cycles). **(B)** Bar diagram showing the stability of the fabricated pDNA/CysFl/Au bioelectrode.

Table 1. The performances of the DNA hybridization detection based on pDNA/CysFl/Au platform compared with other platforms based on other reported hierarchical structures.

Scheme 1

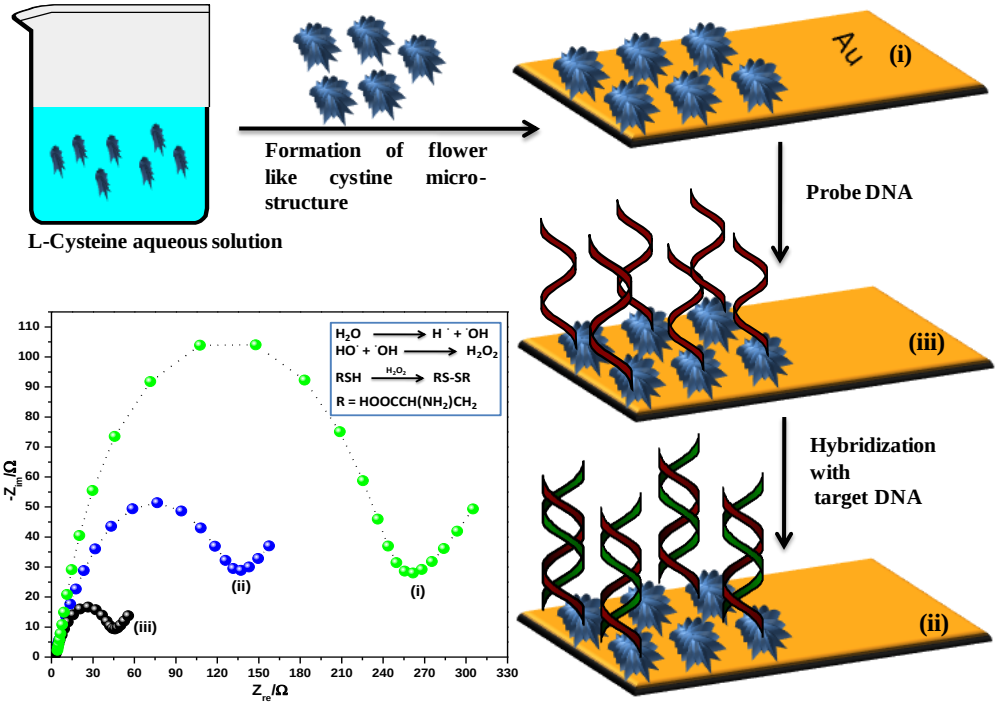

Figure 1

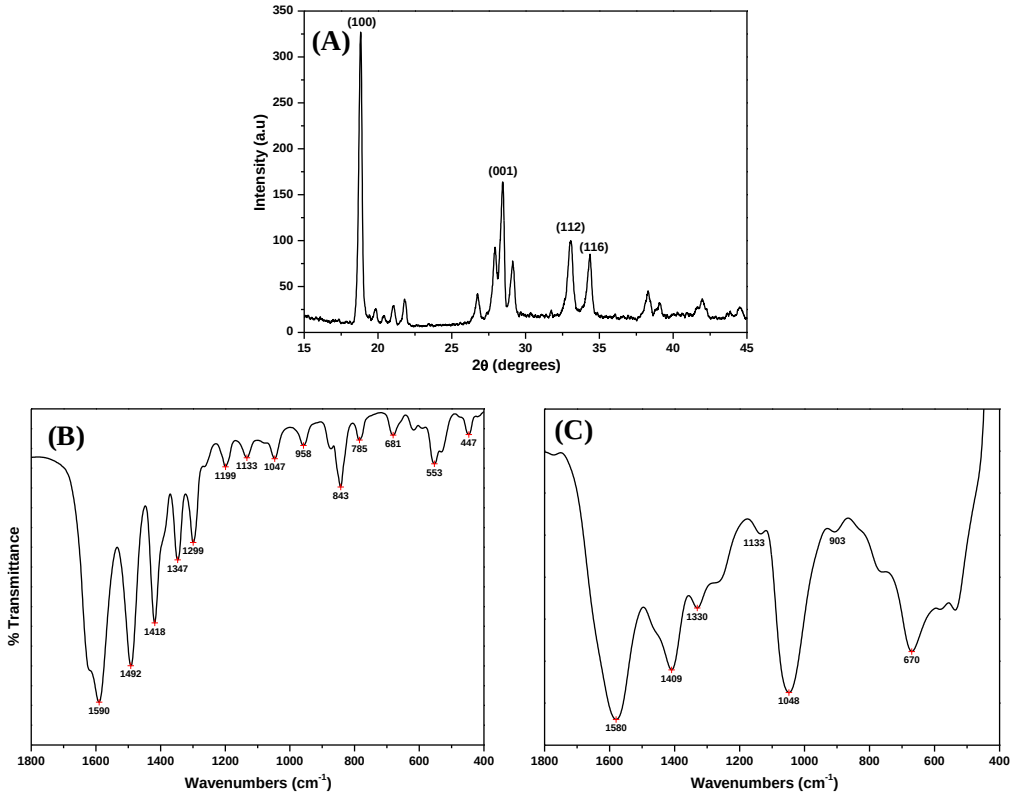

Figure 2

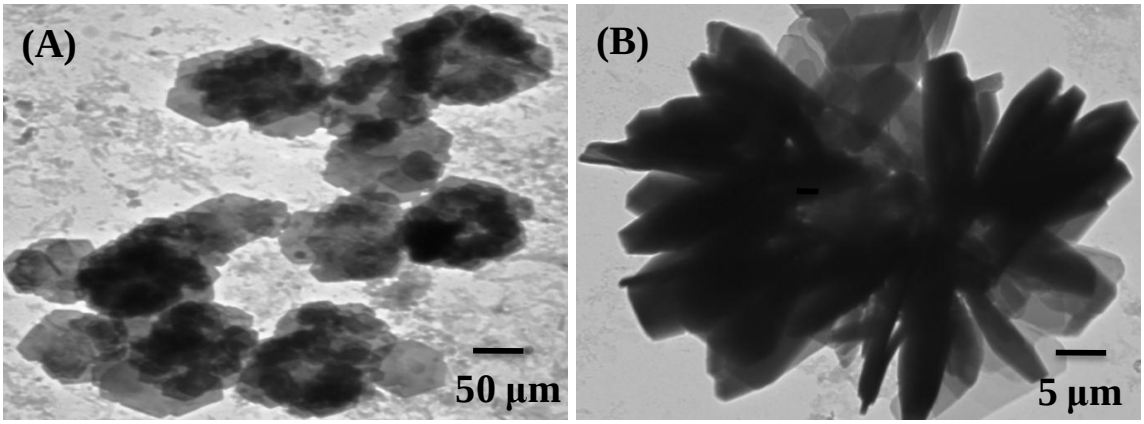

Figure 3

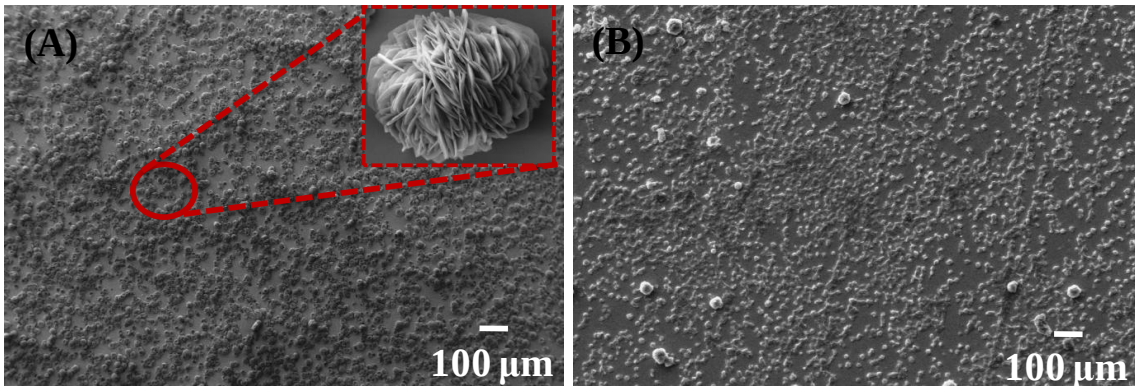

Figure 4

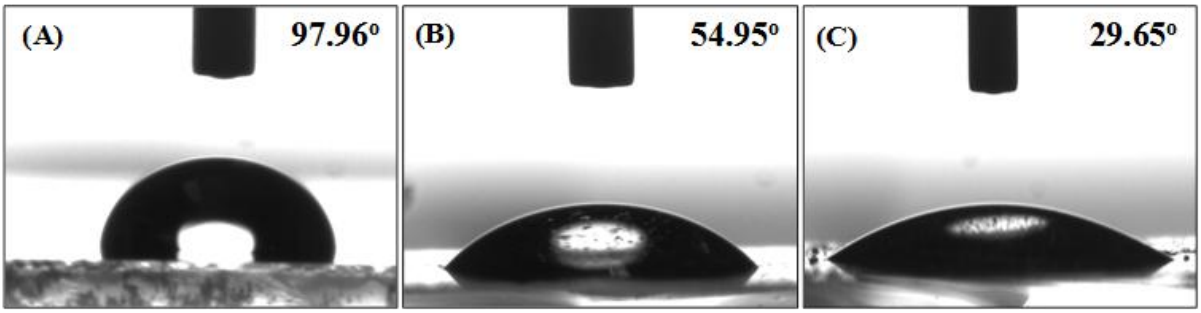

Figure 5

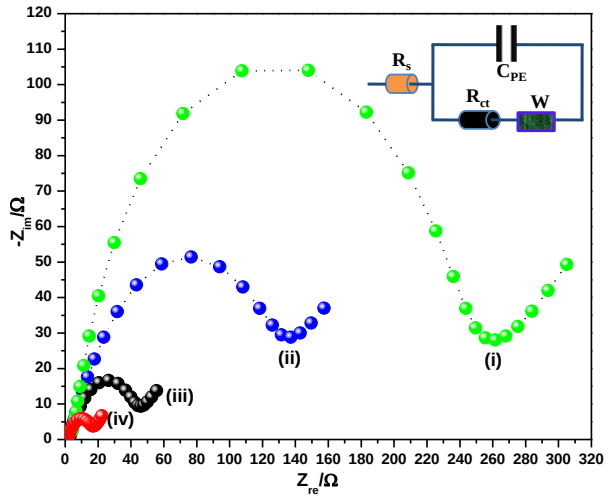

Figure 6

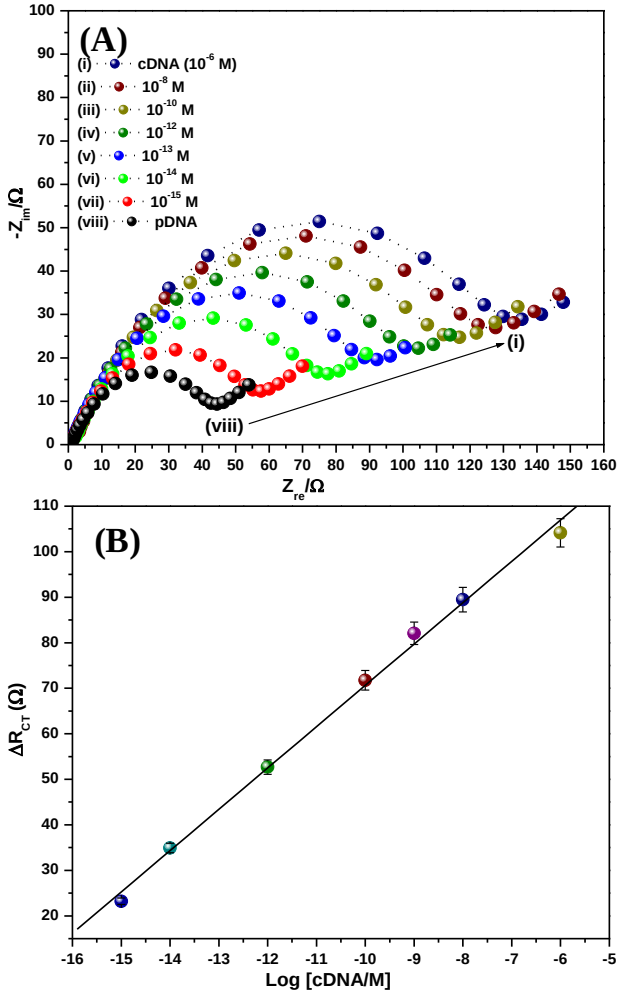

Figure 7

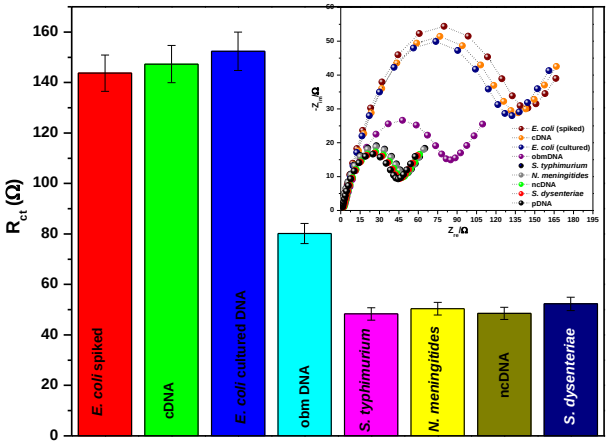

Figure 8

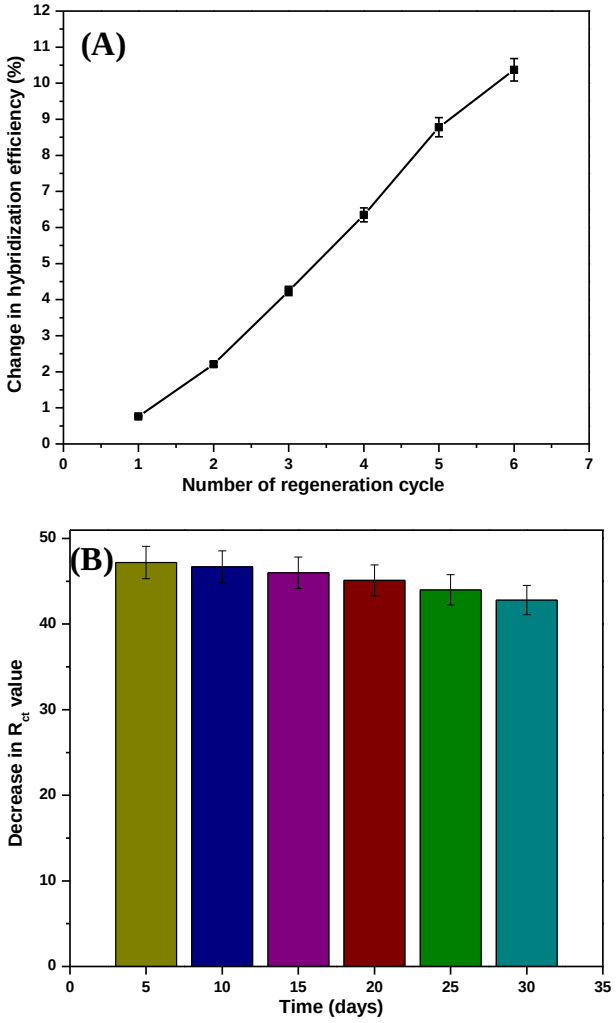

Table 1.

Sl. No	Electrode	Transducer Used	Detection Limit	Detection Range	Reusability	Stability	Ref.
1	Au nanoflower	DPV	1×10^{-12} M	1×10^{-12} – 0.1×10^{-6} M	8 times (15% loss of original signal)	2 weeks (86% of initial response	[27]
2	Polyaniline nanofibres/flower like Au microsphere	EIS	1.9×10^{-14} M	1×10^{-13} – 1×10^{-6} M	6 times (with standard deviation of 3.05%)	10 days (94 % of its initial response)	[42]
3	Au nanoparticle decorated graphene sheets	EIS	3.4×10^{-14} M	1×10^{-13} – 1×10^{-6} M	3 times (loss of original signal 6.04%)	-	[43]
4	Polyaniline nanotube	DPV	1.9×10^{-15} M	3.5×10^{-15} – 755.7×10^{-15} M	2 times (with standard deviation of 3%)	-	[24]
5	dendritic cystine /Au	EIS	0.1×10^{-13} M	1×10^{-14} – 1×10^{-6} M	4 times (signal lost not mentioned)	4 weeks	[33]
6	Cystine nanoflower/Au	EIS	1×10^{-15} M	1×10^{-15} – 1×10^{-6} M	6 times (10.37% signal loss)	30 days (90% of its initial response)	Present Work